Altitude-temporal behaviour of atmospheric ozone, temperature and wind velocity observed at Svalbard

Boyan H Petkov[1], Vito Vitale[1], Tove M. Svendby[2], Georg H. Hansen[2], Piotr S. Sobolewski[3], Kamil Láska[4], Josef Elster[5], Kseniya Pavlova[6], Angelo Viola[1], Mauro Mazzola[1], Angelo Lupi[1], Anna Solomatnikova[6]

[1]Institute of Atmospheric Sciences and Climate (ISAC) of the Italian National Research Council (CNR), Via Gobetti 101, I-40129 Bologna, Italy.

[2]NILU – Norwegian Institute for Air Research, Atmosphere and Climate Department, Instituttveien 18, 2007 Kjeller, Norway.

[3]Institute of Geophysics Polish Academy of Sciences, Department of Atmospheric Physics, Ksiecia Janusza 64, 01-452 Warsaw, Poland.

[4]Department of Geography, Faculty of Science, Masaryk University, Kotlářská 2, CZ-611 37 Brno, Czech Republic

[5]Centre for Polar Ecology, Faculty of Science, University of South Bohemia, Na Zlaté Stoce 3, 37005 České Budějovice and Institute of Botany CAS, CZ-379 82 Třeboň, Czech Republic

[6]Voeikov Main Geophysical Observatory, Laboratory of Ozone Layer Control, Karbysheva str. 7, 194021 St. Petersburg, Russia.

Abstract

The vertical features of the variations in the atmospheric ozone density, temperature and wind velocity observed at Ny-Ålesund, Svalbard were studied by applying the principal component analysis to the ozonesounding data collected during the 1992 – 2016 period. Two data sets corresponding to intra-seasonal (IS) variations, which are composed by harmonics with lower than 1 year periods and inter-annual (IA) variations, characterised by larger periods, were extracted and analysed separately. The IS variations in all the three parameters were found to be composed mainly by harmonics typical for the Madden-Julian Oscillation (from 30- to 60-day periods) and, while the first four principal components (PCs) associated with the temperature and wind contributed about 90% to the IS variations, the ozone IS oscillations appeared to be a higher dimensional object for which the first 15 PCs presented almost the same extent of contribution. The IA variations in the three parameters were consisted of harmonics that correspond to widely registered over the globe Quasi-Biennial, El Niño-Southern, North Atlantic and Arctic Oscillations respectively, and the IA variations turned out to be negligible below the tropopause that characterises the Svalbard troposphere as comparatively closed system with respect to the long-period global variations. The behaviour of the first and second PCs associated with IS ozone variations in the time of particular events, like the strong ozone depletion over Arctic in the spring 2011 and solar eclipses was discussed and the changes in the amplitude-frequency features of these PCs were assumed as signs of the atmosphere response to the considered phenomena.

Keywords: Arctic atmosphere; Variations in atmospheric parameters; Atmospheric ozone; Temperature, ozone, and wind profiles; Ozone depletion; Ozone response to solar eclipse.

1. Introduction

Solar radiation is the main energy source for our planet, which affects variety of chemical and dynamical processes taking place in the upper terrestrial layers. Due to the rotation of the Earth both around its axis and around the Sun, radiation entering the atmosphere is a subject of diurnal, semi-annual and annual oscillations (Iqbal, 1983) that can be recognised also in the temporal behaviour of many geophysical parameters (Yashayaev and Zveryaev, 2001; Mlynczak et al., 2011; Youssouf et al., 2016; Lembo et al., 2017). Examinations of the atmospheric thermodynamic variables and trace gas components, like the ozone, have evidenced on the other hand that except for the induced by solar radiation oscillations, their temporal evolution is characterised by harmonics, which pertain to a very large spectral band extended from daily to decade time scales (Sitnov 1996 and 2004; Goswami and Ajaya Mohan 2001; Ziemke et al., 2007; Lee et al., 2010; Li et al., 2012; Petkov et al., 2012; Henderson et al., 2014; Christiansen et al., 2017). The appearance of these secondary oscillation modes can be considered a result of internal geophysical processes including interactions among the atmosphere, Earth surface and ocean, and hence, their study could contribute to a better understanding of the mechanisms driving the atmospheric dynamics and could enhance the forecasting reliability (Jones et al., 2001; Hollingsworth et al., 2008; Lau and Waliser 2012). However, despite the advantages in this issue, many specific features of the variations remain still far from a clear explanation (Baldwin et al., 2001; Wanner 2001; Zhang 2005; Li et al., 2013, Henderson 2014) that makes their study an important task for the atmospheric science.

According to the nowadays concepts, variety of the oscillations usually observed in the atmospheric parameters turn out to be generated in the tropical regions as a result of the interaction between the ocean and atmosphere and propagate after that toward the extratropical and high latitude areas (Lou 1997; García-Herrera et al., 2006; Fletcher and Kushner, 2011; Flatau and Kim, 2013). Madden-Julian Oscillation (MJO, Madden and Julian 1971; Reid 1994; Zhang 2005; Tian et al., 2007) with periodicities of 30 – 60-day that are considered to be the main mode of the intra-seasonal

variations and El Niño-Southern Oscillation (ENSO, Stenseth et al., 2003; García-Herrera et al., 2006; Wang et al., 2012) characterised by periods from 2 to 10 years, respectively are two important modes of the variations originated in the tropics and persistent over the globe. Quasi-biennial oscillation (QBO, Baldwin et al., 2001), observed in the winds of the equatorial stratosphere that is characterised by a period of about 28 months is another important class of variations recognised also in the behaviour of various atmospheric parameters all over the world (Sitnov, 1996 and 2004; Lee et al., 2010; WMO, 2014; Sofieva et al., 2017). The North Atlantic and Arctic oscillations (NAO and AO, respectively) originate in the higher latitudes of the northern hemisphere (Wanner et al. 2001; Stenseth et al., 2003; Kim et al., 2014) and they are composed by harmonics extended from weekly and longer than seasonal time-scales to approximately 10 years. In addition, the interaction among above listed oscillations, or between one of them and the annual cycle is able to produce variations with intermediate periodicities (Baldwin et al., 2001; Zhou and Miller, 2005; Stuecker et al., 2013). It should be pointed out that the fluctuations in solar activity, which were found to contain spectral components lying from 1- to 100-year periods (Moussas et al., 2005; Lilensten 2007; Hathaway 2015) can also be an external factor, able to impact the variations observed in the atmospheric parameters (Reid, 1991; Svendby and Dahlback, 2004; Haigh, 2007; Solheim et al., 2011; WMO, 2014; Li and Tung, 2014; Fytterer et al., 2015; Steinbrecht et al., 2017).

All these oscillations, induced by dynamical processes that occur in the upper layers of our planet and that are driven by the solar radiation, can be registered at each point of the globe to a different extent of intensity depending on the specific geographical characteristics of the site. On the other hand, the response to these variations indicates how sensitive is the environment of the studied location to the global processes that could contribute to enlargement of our knowledge about the corresponding geographical region. In this context, the evolution of atmospheric parameters in the polar regions, where the winter vortex causes appreciable periodic change in the regional dynamics and the ocean-atmosphere interactions are forced also by the sea-ice cover, appears to be an important issue (Serreze and Barry, 2011; Mitchell et al., 2011; Kim et al., 2014). Such considerations designed

the idea of the present study, aimed to analyse the vertical features of the variations in the atmospheric ozone, temperature and wind velocity, and to give a picture of the spectral composition characterising these variations by examining the data collected from ozonesondes, which were launched at Ny-Ålesund, Svalbard. To achieve this goal, the principal component analysis was applied to the studied data-set in order to outline how the intensities of the variations characterised by different periodicities are distributed in height. Similar approach was applied by Lee et al. (2010) to analyse the QBO observed in the ozone variations registered in the layer between 20 and 28 km altitudes in the tropical regions and by Petkov (2015), who examined the vertical distributions of the variations in the temperature given by radiosondes launched at San Pietro Capofiume station in north Italy from 1987 to 2010. The next section presents the data-sets and shortly describes the method applied for the analyses, while the results are exhibited and discussed in section 3.

2. Datasets and method

Data provided by 2207 ozone soundings launched from 1 January 1992 until 3 August 2016 at Ny-Ålesund (78°56′N, 11°55′E, 11 m amsl), Svalbard by the group of Alfred Wegner Institute, Germany with frequency varying between 1 and 10 days were examined for the purposes of the present analysis. Vaisala RS80, RS90 and RS92 radiosondes equipped with electrochemical concentration cell ozone sensor gave the vertical profiles of atmospheric pressure, relative humidity, temperature, ozone partial pressure and both horizontal wind direction and velocity. Since the type of the ozone sensor together with sensing solution was the same during the period under study, the inhomogeneity of the collected ozone profiles was assumed to be negligible. The thermocap sensor mounted on the RS80 radiosondes is characterised by comparatively high response time at low pressures that leads to significant lag errors in the temperature measurements at upper altitude levels and to minimise such uncertainties, the correction procedure developed by Toamsi et al. (2012) was applied. Figure 1 exhibits the vertical

profiles of the ozone density C_O in molecules per cm^3 (hereinafter referred to as cm^{-3}), temperature T in degree K and horizontal wind velocity V in m s^{-1} taken from the ozonesondes, which were the subject of the following study.

The principal component analysis, adopted to examine the variations of the considered parameters is an approach, widely used in meteorology to study the spatio-temporal evolution of a scalar field presented by an atmospheric parameter and forecasting its behaviour (Björnsson and Venegas, 1997; Camp et al. 2003; Hannachi et al. 2007). The method explores the anomaly matrix $\mathbf{F}$ composed by the deviations ΔX of the variable under study X from its average trend. The spatial distributions of the anomalies $\Delta X(t_i)_j$ over a surface area determined by a grid of $j = 1, 2, \Lambda\ , n$ observational points obtained at fixed times t_i are presented as rows in $\mathbf{F}$, while the columns are uniquely sampled time series for each grid point j composed by the values of anomalies at times $t_i\ (i = 1, 2, \Lambda\ , m)$:

$$\mathbf{F} = \begin{pmatrix} \Delta X(t_1)_1 & \Delta X(t_1)_2 & \Lambda & \Delta X(t_1)_n \\ \Delta X(t_2)_1 & \Delta X(t_2)_2 & \Lambda & \Delta X(t_2)_n \\ \mathrm{M} & \mathrm{M} & \Lambda & \mathrm{M} \\ \Delta X(t_m)_1 & \Delta X(t_m)_2 & \Lambda & \Delta X(t_m)_n \end{pmatrix} \quad . \tag{1}$$

The covariance matrix $\mathbf{C} = [1/(m-1)]\mathbf{F}^{\mathrm{T}}\mathbf{F}$ that is assumed to characterise the variations of the scalar field over the considered area, can be projected onto orthogonal vectors by solving the eigenvalue problem, which projection can also be performed by applying the Singular Value Decomposition (SVD) to the anomaly matrix $\mathbf{F}$. In case of $m > n$, this alternative approach presents $\mathbf{F}$ as a product of three matrices:

$$\mathbf{F} = \mathbf{P}\,\mathbf{S}\,\mathbf{E}^{\mathrm{T}}\ , \tag{2}$$

where the columns of the $m \times n$ matrix **P** are uncorrelated time series named as Principal Components (PCs), while the columns of the $n \times n$ matrix **E** are orthogonal to each other vectors known as Empirical Orthogonal Functions (EOFs). Each EOF_j of the EOFs are considered to represent a basis spatial pattern of the variations in the examined scalar field, while the corresponding PC_j gives the time evolution of this pattern. The diagonal matrix $\mathbf{S} = \left(s_{jj} : s_{11} \geq s_{22} \geq \Lambda \geq s_{nn} \geq 0\right)$ contains the singular values, which allow the estimation of the weight w_j of each *j*-th pair $(EOF, PC)_j$ in the spatio-temporal variations:

$$w_j\left(\text{in } \%\right) = \frac{s_{jj}^2}{\sum_{j=1}^{n} s_{jj}^2} \cdot 100 \ . \tag{3}$$

In practice, only a few of the EOFs and PCs have significant weight w_j and hence, the decomposition performed through Eq. (2) projects the variations presented by *n* time series and *m* spatial maps, respectively onto a space determined by *k* (*k* << *m*, *n*) orthogonal vectors EOFs (maps) and *k* uncorrelated time series (PCs) reducing significantly the dimension of the problem. The cumulative weight

$$W_k = \sum_{j=1}^{k} w_j \tag{4}$$

determined as the sum of the first *k* values of w_j in the most of the real cases rapidly increases to 100% (see Fig. 5 for instance) that provides an estimate of the number *k* ($k : W_k \approx 100\%$) of pairs $(EOF, PC)_j$, which allow a realistic reconstruction of the spatio-temporal variability in the studied parameter.

In the current study this approach was applied to examine the altitude-temporal structure of the variations in the ozone, temperature and wind velocity using their profiles provided by the ozonesondes and taking the height distribution as spatial component. In this case the anomalies,

estimated for each of these variables at *n* altitude levels $z_j\ (j = 1, 2, \Lambda\ , n)$ were taken as rows in the corresponding matrix **F** that assumes the columns as time series representing the temporal evolution of these anomalies at each z_j. The SVD procedure (Eq. 2) was performed by using the corresponding MATLAB function and each EOF was multiplied by the associated singular value and each PC was divided by the same value, respectively that, according to Camp et al. (2003) returns the EOFs in absolute units. In addition, the PCs were subjects of spectral analysis, performed following the Lomb−Scargle [24, 25] periodogram approach in order to study their spectral features and hence, the features of the variability in the studied parameters.

3. Results and discussion

As a first step of the adopted procedure, each profile of the variables under study was interpolated over an altitude grid that starts from the station level (11 m) and increases after that by a step of 100 m from the second level equal to 100 m. It was found that 94% of the ozonesoundings reached an altitude above 20 km, 88% exceeded 25 km, 73% overshoot 30 km and only 16% arrived at altitude higher than 35 km that led us to assume the height of 25 km as the upper border in the present analysis and the altitude grid in this case turns out to contain $n = 251$ levels. The next step was the construction of the data matrix **F′** that, similarly to **F**, contains all the 2207 ozonesoundings as rows and Fig. 2 illustrates the time patterns of the three studied parameters presented as columns of **F′** and corresponding to 15 km altitude. The missing values in each column were filled by linear interpolation and if such a value was at the beginning or at the end of the time series, it was replaced by the average of the column. Since the chosen method requires uniquely sampled time series, each column was additionally interpolated over a time grid presenting a constant discrepancy Δt between the neighbour sampling times. Intervals between the sounding launches were characterised by bimodal distribution indicating that about 70% of the sondes were floated with intervals between 1 and 6 days among the

launches, with a maximum of nearly 18% at 3 days, while approximately 30% pertained to the launch intervals between 6 and 10 days with a peak of about 21% at 7 days. Since the major launching frequency varied from 1 to 6 days the corresponding distribution peak at 3 days was assumed to provide a reasonable sampling step Δt for the second interpolation of the columns in **F′** that acted also as a smoothing, which reduced the amplitudes of the variations with periods lower than 3 days. As a result of the above initial steps, a (2994×251) data matrix **F′** was constructed for each of the three parameters subject of the present analysis.

Figure 2 clearly shows that the annual oscillations are the main mode in the ozone, temperature and wind velocity variations, which turns out to be modulated by both higher- and lower-frequency variations. To perform a precise study of these spectral components it was decided to separate them and the high-frequency band characterised by periods lower than 1 year, hereinafter referred to as intra-seasonal (IS) oscillations according to the common terminology, were analysed separately from the inter-annual (IA) oscillations characterised by periods longer than 1 year. The strong dominating annual oscillations were removed from the examined data and the next subsection presents the construction of the two anomaly matrices corresponding to IS and IA variations for each of the parameters under study, which matrices were the inputs for the SVD approach expressed by Eq. (2).

3.1. Construction of the anomaly matrices.

The filtering of the long-period components from the time series represented by the columns of **F'** was made through running average procedure applied with a 30-day window and repeated 10 times in order to achieve a better effect. The curve in Fig. 3(a) illustrates the result of this smoothing in case of C_O variations observed at 18 km, which was removed from the original data to obtain the anomalies that represent the IS variations in the ozone, exhibited by Fig. 3(b). Following this approach the columns of each matrix **F'** composed from the C_O, T and V data, respectively were elaborated to construct the anomaly matrices $\mathbf{F_{IS}}$ that correspond to the IS variations in the three variables. It should

be pointed out that despite the removal of the seasonal variations from the original data, a modulation of the IS variations by the annual component can be seen in Fig. 3(b) that will be discussed in Subsection 3.3.

The sequence, found as a result of the smoothing was detrended through linear best-fitting over the whole 1992-2016 period that returns the time series, illustrated by the grey curve in Fig. 3(c). The vertical distributions of the trends γ_O, γ_T, γ_V found for each of the time series characterising the behaviour of C_O, T and V respectively, are exhibited in Fig. 4. It is seen that negative ozone trends took place in the boundary layer and in the upper troposphere region, while in the middle troposphere γ_O varied closely around zero and $\gamma_O > 0$ characterised the ozone evolution in the lower stratosphere. The positive trend ranging from 0.5 to 3.5 % dec^{-1} between 10 and 25 km altitudes (Fig. 4(a)) is similar to that given in the WMO report (2014), where an average trend from 0 to 2 % dec^{-1} was found to characterise the ozone behaviour at 60°N after 2000. The temperature trend (Fig. 4(b)) sharply decreased in the boundary layer showing a surface value of nearly 1.6 K dec^{-1} that is consistent with the corresponding value of 1.3±0.7 K dec^{-1}, obtained by Maturilli et al. (2015) from the analysis of the meteorological surface measurements at Ny-Ålesund. In the troposphere and up to about 14 km γ_T shows values varying between 0.4 and 0.8 K dec^{-1}, and gradually decreased after that converting into negative values at altitudes over 20 km. The wind trend γ_V (Fig. 4(c)) exhibited significant oscillations within the layer until 25 km remaining between -0.4 and 0.1 m s^{-1}dec^{-1}.

The grey curve in Fig. 3(c) illustrates detrended long-period variations in the ozone from which the annual cycle together with the shorter period harmonics and noises, given by the black curve in Fig. 3(c) were removed to obtain the anomalies determining the IA oscillations presented in Fig. 3(d). Analogously to the matrices $\mathbf{F_{IS}}$, the corresponding three $\mathbf{F_{IA}}$ anomaly matrices associated with the IA oscillations in C_O, T and V have been constructed and were the subject of the following study.

3.2. Basis profiles (EOFs) of the ozone, temperature and wind variability.

The cumulative weights W_k evaluated by means of Eqs. (3) and (4) for the first 15 pairs (EOF, PC)$_{1\text{-}15}$ resulted from the decomposition of $\mathbf{F_{IS}}$ and $\mathbf{F_{IA}}$ matrices, which were constructed for the three considered atmospheric parameters are shown in Fig. 5. It is seen that the first 4 (EOF, PC)$_{1\text{-}4}$ pairs explain about 70% of the IS ozone variations, while a similar percentage can be achieved considering only the first and second pairs in case of the temperature and wind. For better description of the IS ozone oscillations ($W_k \approx 90\%$), the (EOF, PC)$_{1\text{-}15}$ pairs should be taken into account, while to reach $W_k \approx 90\%$ in case of the other two parameters just the first four components need to be considered that reveals the more complex nature of the IS ozone oscillations, determined by a higher dimensional representation in terms of the decomposition performed by Eq. (2). On the contrary, Fig. 5 shows that a reliable description of the IA variations can be achieved by projecting them onto number of principal components lower than in the case of IS oscillations. In fact, the IA (EOF, PC)$_{1\text{-}2}$ pairs found for C_O, T and V, respectively account for about 80% of the corresponding IA variations and the weight of the first pair concerning the ozone and temperature is about 72%. The first pair associated with the wind velocity shows significantly lower weight of 55% but the common contribution together with the second pair is about 90%. It should be mentioned that (EOF, PC)$_{1\text{-}4}$ explain nearly 93% of the IA variations observed in the three considered parameters.

Figure 6 exhibits the first four EOFs components of the $\mathbf{F_{IS}}$ and $\mathbf{F_{IA}}$ matrices considered main patterns of the studied variations, which can be interpreted as basis profiles showing the vertical distribution of the variation amplitudes that determine the intensity of the oscillations. Each of these profiles EOF$_j$ corresponds to a PC$_j$ that governs the temporal evolution of the studied parameter, so that the variations at certain altitude level z' are composed by 4 basis time series PC$_{1\text{-}4}$ with specific spectral features and the intensity of any basis PC$_j$ is determined by the EOF$_j$(z') value. Bearing in mind these considerations it can be concluded that except for the removed annual cucle, IS

oscillations turn out to play a prevailing role in the variability observed in the three parameters since the corresponding EOFs given in Fig.6 exhibit larger amplitudes in most of the cases. Another important feature of the EOFs that can be seen in Fig. 6 is their layered structure depicted by wave-like forms that outline different altitude trends in the troposphere and stratosphere. As a result of such a behaviour the values of some EOFs at certain altitudes become close to zero that assumes strong reductions of the variations presented by the corresponding PCs at these levels and moreover, there exist heights z_l for which $EOF_j(z_l) = 0$ and hence, the variations with spectral features determined by the corresponding PC_j appear to be completely excluded at z_l. The wave-like structure is also associated with an inversion of the EOF sign at some altitude layers as it is seen in Fig. 6 that can be interpreted as a change of the oscillation phases in these layers.

The upper row of Fig. 6 shows extremely small amplitude of both IS and IA ozone variations in the troposphere that can be accounted for the lower ozone density with respect to upper altitudes. Intensity of the IS ozone variations enhances in the lower stratosphere, showing two maxima at about 10 and 15 km, respectively as can be seen in the upper row of Fig. 6, which indicates that 52% of the IS oscillations, explained by EOF_1 and EOF_2 are bounded between about 7 and 20 km altitudes. This conclusion is consistent with the findings reported by Tian et al. (2007) and Li et al. (2013) who found that the MJO component of the IS variations was manifested mainly in the lower stratosphere. Unlike the ozone, the IS variations in temperature and wind velocity can be registered at all altitude levels considered in the present study. The temperature IS variations in the troposphere are mainly presented by EOF_2, while the EOF_1 oscillations dominate in the lower stratosphere and are contributed also by EOF_3 above 20 km. The IS wind velocity variations determined by EOF_1 and EOF_2 increase with opposite phases in the troposphere reaching a maximum at about the tropopause level, where the polar jet streams usually occur (Archer and Caldeira, 2008).

The first EOFs associated with the IA variations in the ozone, temperature and wind velocity show similar features determined by negligible intensity in the troposphere and an enhancement in the lower stratosphere (Fig. 6). The second EOF of the temperature and wind indicate a slight increase in

the troposphere but, taking into account that the temperature EOF_2 presents much smaller with respect to the EOF_1 weight, it can be assumed that only the wind velocity can be characterised by low intensive IA variations in the troposphere. Hence, bearing in mind that IA oscillations are usually generated by large-scale processes including atmosphere, ocean and sea-ice interactions, the above results allow us to assume a conservative character of the Svalbard troposphere, which remains almost closed for the global IA variations. It should be mentioned that a similar analysis of radiosounding data collected at a middle latitude station in north Italy during 23-year period (Petkov 2015), showed that the temperature IA variations observed in the troposphere were characterised by comparable, or even higher than in the lower stratosphere intensity.

3.3. Spectral features of the ozone, temperature and wind variations.

Figure 7 illustrates the behaviour of the PC_1 components found for the IS and IA variations in the three atmospheric parameters under study, while Figs. 8 and 9 exhibit the spectra of the first four PCs corresponding to the EOFs given in Fig. 6. As can be seen each PC spectrum turns out to be dominated by harmonics p or bands Δp containing specific peaks, which are given in Table 1. Fig. 8 shows that all IS PC spectral components lie mainly between 20- and 120-day periods and the ozone and temperature oscillations appear to be modulated by annual and semi-annual components to different extent. Since the seasonal cycle that could be associated with the oscillations of the incoming solar irradiance was removed from the initial data to obtain the IS variations, the presence of the annual component can be accounted for internal atmospheric process with periodicity of 1 year, like the polar vortex, which is able to impact the ozone and temperature. In fact, as can be seen from Fig. 7, and also from Figs 10, the ozone PC_1 intensity enhances during the boreal winter plausibly due to variation in the strength of the polar vortices. Figure 8 and Table 1 show that harmonics pertaining to the 30 – 60-day spectral range present a significant weight in the IS variations, which confirms the recent findings that MJO, being generated in the tropics is able to modulate the variations in Arctic

atmosphere (L'Heureux and Higgins, 2008; Yoo and Lee, 2011; Li et al., 2013). Except for MJO the 60 – 120-day band also demonstrates significant power in the IS variations, which harmonics could be attributed to local processes interacting with annual and semi-annual cycles.

The PC spectra of the IA variations observed in the three atmospheric parameters under study are shown in Fig. 9 and the corresponding peaks are given in Table 1. The shorter period harmonic peaked at p = 1.1 years can be recognised in the first, second and fourth temperature PCs, and in the $PC_{2\text{-}4}$ associated with the ozone and wind IA variations. It is worth pointing out that this spectral component is close to the period of Chandler wobble found to lie at about 1.2 years and considered the main harmonic of the polar motion (Gross, 2007). QBO is another strongly presented harmonic, identified here as p = 2.4 years (or p = 2.2 years in some of the cases), which component was reported in previous studies (Sitnov, 1996 and 2004; Lee et al., 2010; WMO, 2014; Petkov, 2015; Sofieva et al., 2017), while the periods between 1.4 years and QBO could be considered a result of interaction between QBO and the annual cycles (Baldwin et al., 2001). The oscillations with periods larger than 3 years can be accounted for the ENSO, NAO, AO, Schwabe 11-year solar cycle and their interactions to each other, respectively. Most of these long-period oscillations were registered in the ozone column variations observed at Oslo for the period from 1978 to 1998 by Svendby and Dahlback (2004), who recognised them by using the multiple regression analysis. Bearing in mind that PC_1 explains nearly 70% of the IA variations in ozone and temperature, and PC_1 together with PC_2 contribute about 90% of the IA wind variations it could be concluded from Fig. 9 and Table 1 that QBO, ENSO, NAO and AO turn out to dominate the IA variations of all the three parameters under study. The 24-year cycle detected in the PC_1 ozone and PC_3 temperature IA variations, together with the 12-year oscillations found in the PC_3 ozone, PC_2 temperature and wind, and PC_4 wind components could be associated with the solar activity cycles (22- and 11-year, respectively). It should be pointed out that the variations in solar activity was found to contain long period components, for instance 80 – 90-year or longer (Hathaway 2015) and hence, these periodicities could be also observed in the behaviour of the atmospheric variables. However, the studied time series are too short to detect similar harmonics but

the hypothesis that the trends given in Fig. 4 appear to be segments of such periodicities cannot be excluded.

The spectral features of variations in ozone, temperature and wind velocity at different altitude levels in the Svalbard atmosphere show that except for the spectral components of the incoming solar radiation considered the main forcing factor, the presence of various other harmonics that are not multiples of those in the solar radiation can be observed, which is a typical characteristic of a complex chaotic system (Anishchenko et al., 2007).

3.4. Response of the IS ozone variation to particular events.

As pointed out in Section 1, the variations observed in atmospheric parameters can be considered a result of the oscillations in the incoming solar radiation on the one hand and, an effect of processes involving both atmosphere and ocean, on the other hand. In this context, a response of the variations to particular internal atmospheric events or to external episodes that disturb the incoming solar radiation could be assumed and such a concept is discussed below making use of the IS ozone variations analysed in the previous subsection.

The polar vortex is a specific winter phenomenon in Arctic that is able to disturb the ozone behaviour intensifying the ozone destruction processes in the stratosphere. The extremely cold polar vortex occurred in the 2010/2011 winter caused the deepest ozone depletion registered until now in Arctic, which was observed at Ny-Ålesund in the second half of March. Moreover, this strong depletion episode was found to affect significantly the ozone column at lower latitudes, as well (Petkov et al., 2014 and references therein). Figure 10 shows time patterns of PC_1 and PC_2 IS ozone variations for the time from 2010 to 2013, where changes in the amplitude-frequency characteristics after the ozone depletion event could be recognised. To examine such an appearance, the spectra of

the PC_1 were evaluated for the period from September 2010 to February 2011* on the one hand and from April to September 2011, on the other hand, and the results are shown in Fig. 11. The length of these two time-intervals was chosen to be 6 months in order to achieve reasonable covering of the times before and after the event with segments, sufficiently long to allow the detection of the main IS spectral components presented in Fig. 8 and Table 1. The first interval spreads before and during the vortex occurrence, while the second interval starts with the destruction of the vortex and lasts several months after that. As can be seen from Fig. 11, the harmonic at $p = 60$ days, which is the major component before the event, turns out to be strongly reduced after that, while the amplitude $A(p)$ for p = 35 shows an increase. Comparatively lower reduction can be also marked in the 25-day component, while the short-period band is a subject of significant change in the second period characterised by a decrease in the amplitude of the harmonics p < 12 days. To check if such modifications in the amplitude-frequency features took place also for all the years considered in the present study, a similar spectral analysis was made for any 6-month time-interval T_i' that starts from September of each year i (i = 1992, …, 2014) and lasts to February of the next year i+1 on the one hand, and for the time-interval T_{i+1}'' from April to September of the year i+1, on the other hand. Figure 12 exhibits the time patterns of the amplitudes $A_i'(p)$ and $A_{i+1}''(p)$ that correspond to the three spectral components, peaked at 60-, 35- and 25-day periods and which were calculated for T_i' and T_{i+1}'', respectively. The two values $A_i'(p)$ and $A_{i+1}''(p)$ given in Fig. 12 for each year i are connected with a line, so that the distance between these two points $|A_i'(p) - A_{i+1}''(p)|$ illustrates the change in the corresponding amplitude for the time before and after the polar vortex. It is seen that the considered amplitudes were subjects of both decreases and increases passing from the first to the second time intervals and the magnitude of such a change vary from year to year. Figure 12(a) shows that the discrepancy $|A_i'(60) - A_{i+1}''(60)|$ predominantly increased after 2005 and the largest value reaching

* Here and henceforth the first day of the initial month and the last day of the final month that bound the time-intervals chosen for determining the amplitude of the corresponding harmonics will be omitted for the sake of simplicity.

about an order of magnitude took place during the 2010/2011 period that corresponds to a strong abatement of the harmonic p = 60 days shown in Fig. 11. Similarly, the amplitude discrepancy $|A'_i(35) - A''_{i+1}(35)|$ exhibited in Fig. 12(b) presents a maximum increase for the same time, which increase gradually reduces within the next two years. It should be pointed out that the amplitude of the 25-day component, given in Fig. 12(c) shows a significant decrease passing from T'_{2009} to T''_{2010}, or one year before the event. These results indicate that some spectral components of the PC_1 ozone variations like those at p = 60 and p = 35 days, which correspond to the MJO, changed in the time of the 2011 ozone depletion event more markedly than within the whole period under study. Similar analysis, performed for the short-period components (p < 12 days) of the IS ozone PC_1 variations, shown in Fig. 11, was not able to bring us to an analogous inference.

Summarising, it could be concluded that specific dynamical events, which occurred in the polar atmosphere, could affect MJO components of the IS ozone variations at Ny-Ålesund that assumes an important role of the regional factors for this spectral band despite that MJO are considered as being modulated by tropical processes (Li et al., 2013 and references therein). The significant amplitude decrease of the 25-day harmonic pertaining to the PC1 ozone oscillations after the 2009/2010 polar vortex, or one year before the strongest ozone depletion (see Fig. 12(c)), is worthy of noticing as an eventual sign for the further event that needs a careful analysis far beyond the scope of this study.

The solar eclipse is another particular event that causes a disturbance in the regular variability of the incoming solar radiation, which is being assumed a pacemaker for various processes in the atmosphere-ocean-surface system. Sixteen solar eclipses occurred over the north hemisphere during the examined period but only in five of them, listed in Table 2, the Moon umbra and penumbra covered large areas extended from tropical and mid- until high-latitudes, including also Svalbard. Figure 13 exhibits the behaviour of the ozone PC_2 IS variations for periods including some of the eclipses given in Table 2. It is seen that similarly to the case of the ozone depletion event, the amplitude-frequency characteristics of PC_2 variations appear to change passing through the days of

the eclipses and such a change lasted sometimes for a comparatively long time. For instance, Fig. 13(a) shows that after the 1999 eclipse the amplitude of the PC_2 variations remained almost the same until the end of 2000, without the enlargement usually observed from winter to spring, as can be seen in Fig. 13 in the time before and well after the eclipses. Intensity of the ozone oscillations presented by PC_2 enhanced in the period from October 2005 until March 2006, between the two eclipses (Fig. 13(b)), while immediately after the second, the variations decreased significantly as occurred also in 2008 (Fig. 13(c)). These apparent modifications in the amplitude-frequency features of the PC_2 variations were examined by applying an approach, similar to that used in the case of ozone depletion event. However, since the eclipse occurrences do not present a periodicity like the polar vortex, it was decided to take into account the PC_2 spectra for 6-month intervals starting from January 1992 and Fig. 14 presents the behaviour of the amplitudes associated with 60-, 35- and 25-day harmonics for each half-yearly interval from 1992 to 2015. Figure 14(b) exhibits a sharp decrease in the amplitude of 35-day spectral component that took place immediately after the 1999 eclipse followed by a period of fairly stable level until the next, 2003 eclipse, when a significant increase in the second half of 2003 was registered. The amplitude of the 60-day harmonic decreased after the 1999 eclipse to a lower then 35-day extent (Fig. 14(a)) and it showed extremely large variations between 2003 and 2008, especially around the two close to each other eclipses of 2005 and 2006. It is worth mentioning that similar large variations between 2005 and 2007 were detected also in the 60-day PC_1 component as can be seen in Fig. 12(a) despite the different beginning of the 6-month intervals assumed to estimate the PC_1 harmonic amplitudes. The 25-day amplitude exhibited in Fig. 14(c) largely varied within 2003 – 2009 period, when four of the considered eclipses took place and a sharp decrease was registered after the last eclipse. These examples indicate that significant changes in the amplitudes of harmonics composing the PC_2 IS ozone variations followed eclipse occurrences in some of the cases despite that the extent of such changes does not show similar features for all the eclipses. A plausible explanation of the various response features could be achieved considering the atmospheric ozone in the polar regions as a component of a low dimensional chaotic system (Petkov et al., 2016). An

essential characteristic of this class dynamical systems is the high sensibility to the initial conditions, in other words, the evolution of the system is well determined, so that starting from an arbitrary state chosen as initial, after some time the system should reach a known final state but a small deviation in the initial state is able to lead to an appreciable deviation from the final one. Under this concept, the different responses of the IS ozone variations to the eclipses can be attributed to the different states of the system containing the ozone as a component, before the phenomena. Such a conclusion could be able to shed light on some contradictory results about the effect of the solar eclipse on the ozone obtained in various studies, which reported both increase and decrease (Bojkov, 1968; Gerasopoulos et al., 2008; and references therein) in the ozone column during the event.

4. Conclusions

The variations in the ozone density, temperature and wind velocity were studied by applying the principal component analysis to data-sets provided by ozonesonde measurements carried out at Ny-Ålesund, Svalbard, in order to gain information about the vertical distribution of intensity characterising the oscillation in the three parameters. To achieve this goal, the variations composed by harmonics with periods lower than 1 year, referred to as intra-seasonal (IS) component and those with periods higher than a year, inter-annual (IA) variations respectively, were examined separately. Analysis of the empirical orthogonal functions (EOFs), interpreted as profiles of the variation amplitudes and corresponding principal components (PCs) representing both types of variations showed that the intensity of IS oscillations were higher than IA oscillations. Generally, the vertical distribution of the variations in the studied parameters showed layered wave-like structure, characterised by different amplitude and phase features in the layers, and in the most of the cases the tropopause turned out to be the main layer border. It was found that the IS oscillations were dominated by MJO together with oscillations composed by harmonics from 60- to 120-day periods, while the

spectral composition of the IA component contains harmonics typical for QBO, ENSO, 11- and 22-year solar cycles. Both IS and IA ozone variations are presented mainly in the low stratosphere, where the IS mode is bounded predominantly between 7 and 20 km altitude. Similarly, the IA variations in the temperature and wind velocity showed minor intensity in the troposphere that allows the conclusion about conservative character of the Svalbard troposphere toward the long-period global oscillations. It was found also that a reasonable representation of the IS ozone variations could be achieved by using the first 15 (EOF, PC) pairs, while for the temperature and wind velocity only the first 4 pairs were needed that reveals more complex nature of the ozone density variations.

The behaviour of the IS ozone oscillations in the time of particular events, like the deep ozone depletion occurred in the spring 2011 and solar eclipses, was examined and changes in the amplitude-frequency features of the corresponding PC_1 and PC_2 components were recognised. The spectral analysis of the variations taken within 6-month time-intervals referred to the time before and after the 2011 event showed that the spectral components at 35- and 60-day periods, which are typical for MJO were subject of the largest change with respect to the similar time-intervals chosen for the other years, while a change in the 25-day component took place one year before the event. Analogous modifications in the amplitude-frequency characteristics of PC_2 IS ozone variations were observed in the time of some solar eclipses occurred during the period under study.

Acknowledgements:

The radio and ozone sonde data were provided by the Alfred Wegener Institute, Helmholtz Centre for Polar and Marine Research, and were partly funded from the European Community's Seventh Framework Programme (FP7/2007 - 2013) under grant agreement № 603557 (StratoClim). This research was developed under the Atmosphere Flagship Programme in Ny-Ålesund (http://nysmac.npolar.no/research/flagships/atmosphere.html) as a part of the RiS 10871 "UV

Intercomparison and Integration in a High Arctic Environment (UV-ICARE)" and 3305 "Ultraviolet Irradiance Variability in Arctic (U-VIVA)" projects. The Czech team activity was supported by the NILU - Norwegian Institute for Air Research, № 270644/E109 and also by the Ministry of Education, Youth and Sports of the Czech Republic, № LM2015078 - CzechPolar2, № CZ.02.1.01/0.0/0.0/16_013/0001708 - ECOPOLARIS and by the institutional long-term research plan № RVO 67985939 of the Institute of Botany CAS.

References:

Anishchenko, V.S, Astakhov, V., Neiman, A., Vadivasova, T., Schimansky-Geier, L., 2007. Nonlinear Dynamics of Chaotic and Stochastic Systems (Second edt). Springer, 446 p.

Archer, C. L., Caldeira, K., 2008. Historical trends in the jet streams. Geophys. Res. Lett., 35, L08803.1

Baldwin M. P., Gray, L. J., Dunkerton, T. J., Hamilton, K., Haynes, P.H., Randel, W.J., Holton, J.R., Alexander, M.J., Hirota, I., Horinouchi, T., Jones, D.B.A., Kinnersley, J.S., Marquardt, C., Sato, K., Takahashi M., 2001. The quasi-biennial oscillation, Reviews of Geophysics, 39, 179–229.

Björnsson H., Venegas, S.A., 1997. A manual for EOF and SVD analyses of climatic data, Report № 97-1, Montreal, Quebec.

Bojkov R. D. 1968. The ozone variations during the solar eclipse of 20 May 1966. Tellus, 20, 417 – 421.

Camp C.D., Roulston, M. S., Yung, Y. L., 2003. Temporal and spatial patterns of the interannual variability of total ozone in the tropics, J. Geophys. R., vol. 108(D20), 4643.

Christiansen B, Jepsen, N., Kivi, R., Hansen, G., Larsen, N., Korsholm, U. S., 2017. Trends and annual cycles in soundings of Arctic tropospheric ozone. Atmos. Chem. Phys., 17, 9347–9364.

Fletcher, C. G., Kushner, P. J., 2011. The role of linear interference in the annular mode response to tropical SST forcing, J. Clim. 24, 778–794.

Flatau M, Kim, Y.-J., 2013. Interaction between the MJO and Polar Circulations, Journal of Climate, vol. 26, 3562 – 3574.

Fytterer, T., Mlynczak, M. G., Nieder, H., Pérot, K., Sinnhuber, M., Stiller, G., Urban, J., 2015. Energetic particle induced intra-seasonal variability of ozone inside the Antarctic polar vortex observed in satellite data, Atmos. Chem. Phys., 15, 3327–3338.

García-Herrera R., Calvo, N., Garcia, R. R., Giorgetta, M. A., 2006. Propagation of ENSO temperature signals into the middle atmosphere: a comparison of two general circulation models and ERA-40 reanalysis data, J. Geophys. Res., 111, no. 6, D06101.

Gerasopoulos E., Zerefos, C. S., Tsagouri, I., Founda, D., Amiridis, V., Bais, A. F., Belehaki, A., Christou, N., Economou, G., Kanakidou, M., Karamanos, A., Petrakis, M., Zanis, P., 2008. The total solar eclipse of March 2006: overview, Atmos. Chem. Phys., 8, 5205–5220.

Goswami, B.N., Ajaya Mohan, R.S. 2001. Intraseasonal Oscillations and Interannual Variability of the Indian Summer Monsoon, Journal of Climate, 14, 1180 – 1198.

Gross, R. S., 2007. Earth Roation Variations – Long Period, in Physical Geodesy, edited by T. A. Herring, Treatise on Geophysics, Vol. 11, Elsevier, Amsterdam.

Hannachi A., Jolliffe, I. T., Stephenson, D. B., 2007. Empirical orthogonal functions and related techniques in atmospheric science: A review, International Journal of Climatology, vol. 27, pp. 1119–1152.

Hathaway D. H., 2015. The solar cycle, Living Rev. Solar Phys., 12, 4.

Haigh J. D., 2007. Solar variability and climate, in Space weather. Research towards applications in Europe (Jean Lilensten ed), Springer, 65 – 82.

Henderson, G.R, Barrett, B. S., Lafleur, D. M., 2014. Arctic sea ice and the Madden–Julian Oscillation (MJO), Clim. Dyn., 43, 2185–2196.

Hollingsworth, A., Engelen, R. J., Textor, C., Benedetti, A., Boucher, O., Chevallier, F., Dethof, A., Elbern, H., Eskes, H., Flemming, J., Granier, C., Kaiser, J. W., Morcrette, J.-J., Rayner, P., Peuch, V.-H., Rouil, L., Schultz, M. G., Simmons, A. J., and the GEMS consortium, 2008. Toward a monitoring and forecasting system for atmospheric composition: The GEMS Project, Bull. Am. Meteorol. Soc., 89, 2008, 1147–1164.

Iqbal, M., 1983. An introduction to solar radiation. Academic Press, 390 p.

Jones, P.D., Osborn, T. J., Briffa, K. R., 2001. The Evolution of Climate Over the Last Millennium, Science 292, 662 – 667.

Kim, B.-M., Son, S.-W., Min, S.-K-, Jeong, J.-H., Kim, S.-J., Zhang, X., Shim, T., Yoon, J.-H., 2014. Weakening of the stratospheric polar vortex by Arctic sea-ice loss, Nature Communications, 5, 4646, DOI: 10.1038/ncomms5646.

L'Heureux, M.L., Higgins, R., 2008. Boreal winter links between the Madden–Julian Oscillation and the Arctic Oscillation, J. Clim. 21, 3040–3050

Lau N.-C., 1997. Interactions between global SST anomalies and the midlatitude atmospheric circulation, Bull. Am. Meteorol. Soc., 78, 21–33.

Lau W. K. M., Waliser, D. E., 2012. Intraseasonal Variability in the atmosphere–ocean climate system, (second edition), Springer, Heidelberg, Germany, 646.

Lee, S., Shelow, D. M., Thompson, A. M., Miller, S. K., 2010. QBO and ENSO variability in temperature and ozone from SHADOZ, 1998–2005, J. Geophys. Res., 115, D18105.

Lembo V., Bordi, I., Speranza, A., 2017. Annual and semiannual cycles of midlatitude near-surface temperature and tropospheric baroclinicity: reanalysis data and AOGCM simulations. Earth Syst. Dynam., 8, 295–312.

Li K.-F., Tian, B., Waliser, D. E., Schwartz, M. J., Neu, J. L., Worden, J. R., Yung, Y. L., 2012. Vertical structure of MJO-related subtropical ozone variations from MLS, TES, and SHADOZ data, Atmos. Chem. Phys., 12, 425–436.

Li, K.-F., Tian, B., Tung, K.-K., Kuai, L., Worden, J. R., Yung, Y. L., Slawski, B. L., 2013. A link between tropical intraseasonal variability and Arctic stratospheric ozone, J. Geophys. Res., 118, 4280–4289.

Li, K.-F., Tung, K.-K. 2014. Quasibiennial oscillation and solar cycle influences on winter Arctic total ozone, J. Geophys. Res. Atmos., 119, 5823–5835.

Lilensten J. (Editor, 2007) Space weather, Springer, 331 pages.

Lomb N. R., 1096. Least-squares frequency analysis of unequally spaced data, Astrophysics and Space Sciences, vol. 39, pp.447–462.

Madden, R. A., Julian, P. R., 1971. Detection of a 40-50 day oscillation in the zonal wind in the tropical Pacific, Journal of the Atmospheric Sciences, vol. 28, pp. 702 – 708.

Maturilli M, Herber, A., König-Langlo, G., 2015. Surface radiation climatology for Ny-Ålesund, Svalbard (78.9° N), basic observations for trend detection, Theor. Appl. Climatol. 120, 331–339.

Mitchel, D. M., Gary, L. J. Charlton-Perez, A. J., 2011. The structure and evolution of the stratospheric vortex in response to natural forcings, J. Geophys. Res., 116, D15110, doi:10.1029/2011JD015788.

Mlynczak, P. E., Smith, G. L., Doelling, D. R., 2011. The Annual Cycle of Earth Radiation Budget from Clouds and the Earth's Radiant Energy System (CERES) Data. Journal of Applied Meteorology and Climatology, 50, 2490 – 2503.

Moussas X., Polygiannakis, J.M., Preka-Papadema, P., Exarhos G., 2005. Solar cycles: A tutorial, Advances in Space Research, 35, 725–738.

Petkov B. H., 2015. Temperature variability over the Po Valley, Italy, according to radiosounding data, Advances in Meteorology, Article ID 383614, 9 pages.

Petkov B., Vitale, V., Gröbner, J., Hülsen, G., De Simone, S., Gallo, V., Tomasi, C., Busetto, M., Barth, V. L., Lanconelli, C., Mazzola, M., 2012. Short-term variations in surface UV-B irradiance and total ozone column at Ny-Ålesund during the QAARC campaign, Atmospheric Research, 108, 9–18.

Petkov B. H., Vitale, V., Tomasi, C., Siani, A. M., Seckmeyer, G., Webb, A. R., Smedley, A. R. D., Casale, G. R., Werner, R., Lanconelli, C., Mazzola, M., Lupi, A., Busetto, M., Diémoz, H., Goutail, F., Köhler, U., Mendeva, B. D., Josefsson, W., Moore, D., Bartolomé, M. L., González, J. R. M., Mišaga, O., Dahlback, A., Tóth, Z., Varghese, S., De Backer, H., Stübi, R., Vaníček. K., 2014. Response of the ozone column over Europe to the 2011 Arctic ozone depletion event according to ground-based observations and assessment of the consequent variations in surface UV irradiance, Atmospheric Environment, 85, 169–178.

Petkov B. H, Vitale, V., Mazzola, M., Lanconelli, C., Lupi, A., 2015. Chaotic behaviour of the short-term variations in ozone column observed in Arctic, Communications in Nonlinear Science and Numerical Simulation, 26, 238–249.

Reid G. C., 1991. Solar Total irradiance variations and the global sea surface temperature record, J. Geophys. Res., 96, 2835-2844.

Reid G. C., 1994. Seasonal and interannual temperature variations in the tropical stratosphere, J. Geophys. Res., 99, 18923–18932.

Scargle J. D., 1982. Studies in astronomical time series analysis. II. Statistical aspects of spectral analysis of unevenly spaced data, Astrophysical Journal, vol. 263, pp.835–853.

Serreze M.C., Barry R.G., 2011. Processes and impacts of Arctic amplification: A research synthesis. Global and Planetary Change, 77, 85–96.

Sitnov S.A., 1996. Vertical structure of the extratropical quasi-biennial oscillation in ozone, temperature, and wind derived from ozonesonde data. J. Geophys. Res., 101, 12855-12866.

Sitnov S.A., 2004. QBO effects manifesting in ozone, temperature, and wind profiles, Annales Geophysicae, 22, 1495–1512.

Sofieva, V.F., Kyrölä, E., Laine, M., Tamminen, J, Degenstein, D., Bourassa, A., Roth, C., Zawada, D., Weber, M., Rozanov, A., Rahpoe, N., Stiller, G., Laeng, A., von Clarmann, T., Walker, K. A., Sheese, P., Hubert, D., van Roozendael, M., Zehner, C., Damadeo, R., Zawodny, J., Kramarova, N., Bhartia, P. K., 2017. Merged SAGE II, Ozone_cci and OMPS ozone profile dataset and evaluation of ozone trends in the stratosphere, Atmos. Chem. Phys., 17, 12533–12552.

Solheim, J.-E., Stordahl, K., Humlum, O., 2011, Solar activity and Svalbard temperatures. Advances in Meteorology, 2011, ID 543146.

Steinbrecht, W, Froidevaux, L., Fuller, R., Wang, R., Anderson, J., Roth, C., Bourassa, A., Degenstein, D., Damadeo, R, Zawodny, J., Frith, S., McPeters, R., Bhartia, P., Wild, J., Long, C., Davis, S., Rosenlof, K., Sofieva, V., Walker, K., Rahpoe, N., Rozanov, A., Weber, M., Laeng,

A., von Clarmann, T., Stiller, G., Kramarova, N., Godin-Beekmann, S., Leblanc, T., Querel, R., Swart, D., Boyd, I., Hocke, K., Kämpfer, N., Barras, E.M., Moreira, L., Nedoluha, G., Vigouroux, C., Blumenstock, T., Schneider, M, García, O., Jones, N., Mahieu, E., Smale, D., Kotkamp, M, Robinson, J., Petropavlovskikh, I., Harris, N., Hassler, B., Hubert, D., Tummon F., 2017. An update on ozone profile trends for the period 2000 to 2016, Atmos. Chem. Phys., 17, 10675–10690.

Stenseth N. C., Ottersen, G., Hurrell, J. W., Mysterud, A., Lima, M., Chan, K.-S., Yoccoz, N. G., Ådlandsvik, B., 2003. Studying climate effects on ecology through the use of climate indices: The North Atlantic Oscillation, El Niño Southern Oscillation and beyond (Review), Proceedings of the Royal Society of London B, 270, 2087–2096.

Stuecker M. F., Timmermann, A., Jin, F.-F., McGregor, S., Ren, H.-L., 2013. A combination mode of the annual cycle and the El Niño/Southern Oscillation, Nature Geoscience, 6, 540–544.

Svendby, T. M., Dahlback, A., 2004. Statistical analysis of total ozone measurements in Oslo, Norway, 1978–1998, J. Geophys. Res., 109, D16107.

Tian, B., Yung, Y. L., Waliser, D. E., Tyranowski, T., Kuai, L., Fetzer, E. J., Irion, F. W., 2007. Intraseasonal variations of the tropical total ozone and their connection to the Madden-Julian Oscillation, Geophys. Res. Lett., 34, L08704.

Tomasi C., Petkov B. H., Benedetti, E., 2012. Annual cycles of pressure, temperature, absolute humidity and precipitable water from the radiosoundings performed at Dome C, Antarctica, over the 2005–2009 period, Antarctic Science, v 24, 637 – 658.

Wang C., Deser, C., Yu, J.-Y., DiNezio, P., Clement, A., 2012. “El Niño and southern oscillation (ENSO): a review,” in Coral Reefs of the Eastern Pacific, pp. 3–19.

Wanner H., Brönnimann, S., Casty, C., Gyalistras, D., Luterbacher, J., Schmutz, C., Stephenson, D. B., Xoplaki, E., 2001. North Atlantic oscillation − concepts and studies, Surveys in Geophysics, vol. 22, 321–382, 2001.

WMO, 2014. Scientific assessment of ozone depletion: 2014. World Meteorological Organization, Report No. 55. World Meteorological Organization, Geneva.

Yashayaev, I. M., Zveryaev, I. I., 2001. Climate of the seasonal cycle in the North Pacific and the North Atlantic oceans, Int. J. Climatol. 21: 401–417.

Yoo C, Feldstein, S. B., Lee, S., 2011. The impact of the Madden–Julian Oscillation trend on the Arctic amplification of surface air temperature during the 1979–2008 boreal winter, Geophys. Res. Lett. 38, L24804.

Youssouf M.O., Laurent M., Xavier C., 2016. Statistical Analysis of Sea Surface Temperature and Chlorophyll-a Concentration Patterns in the Gulf of Tadjourah (Djibouti). J. Marine Sci. Res. Dev. 6, 1000186.

Ziemke J.R., Chandra, S., Schoeberl, M. R., Froidevaux, L., Read, W. G., Levelt, P. F., Bhartia, P. K., 2007. Intra-seasonal variability in tropospheric ozone and water vapor in the tropics, J. Gheophys. Res., 34, L17804.

Zhang, Ch., 2005. Madden-Julian Oscillation, Reviews of Geophysics, vol. 43, RG2003.

Zhou, S., Miller, A. J., 2005. The interaction of the Madden–Julian Oscillation and the Arctic Oscillation, Journal of climate, vol. 18, pp. 143 – 159, 2005.

Table 1. The main spectral components p of the first four IS and IA PCs. The symbol "~" indicates a short spectral band Δp centred at the corresponding harmonic p, while the spectral intervals are defined by the bounding harmonics p connected through "-". The semi-annual and annual cycles are denoted as p_{sa} and p_a, respectively. The IA peaks with powers lower than the half of the maximal harmonic are considered to have a minor importance and are given in parenthesis.

PC	IS spectral components (days)			IA spectral components (years)		
	Ozone density C_O	Temperature T	Wind velocity V	Ozone density C_O	Temperature T	Wind velocity V
1	~30, 45-70, p_a	50-120, p_a	25, 30-100	2.4, 3.0, 4.8, 24	1.1, 1.4, 2.4, 3.4 (8.0)	3.4 (8.0)
2	25, 30, ~40, 55-80, p_{sa}, p_a	~48, ~60, ~70, p_{sa}, p_a	40-85, 120	1.1, 2.7, 4.0, (1.7, 8.0)	1.1, 1.8, 12.0 (2.2, 3.4, 6.0)	1.1, 1.3, 2.2, 12.0 (3.0, 6.0)
3	22, 40-120, 150, p_{sa}	~40, ~55, 60-100, p_{sa}	25-90, 120	1.1, 2.4-4.0, 12.0	1.7, 24.0	1.1-1.8, 2.2, 3.0, 6.0
4	25, 30, 40, 50, 80-100, 120, p_{sa}	~30, ~40, 60	25-60, 100	1.1, 1.6, 3.0 (2.4, 8.0)	1.1, 1.4, 2.4-3.0, 6.0-8.0	1.1, 2.4, 3.4, 12.0 (6.0)

Table 2. Some characteristics of the solar eclipses considered in the present study taken from the EmapWin Ver. 1.21 software (Shinobu Takesako, http://www2c.biglobe.ne.jp/~takesako/cal/emapwin_eng_1.21.htm).

Eclipse occurrence and type	11 August 1999 Central total eclipse	31 May 2003 Central annular eclipse	03 October 2005 Central annular eclipse	29 March 2006 Central total eclipse	01 August 2008 Central total eclipse
First umbra contact (Time and location)	09:30 UT 64°54'W, 40°54'N	03:45 UT 04°42'W, 56°54'N	08:41 UT 38°30'W, 47°54'N	08:34 UT 37°00'W, 06°30'S	09:21 UT 101°18'W, 67°54'N
Last umbra contact (Time and location)	12:36 UT 87°06'E, 17°24'N	04:32 UT 60°06'W, 67°54'N	12:22 UT 82°18'E, 09°54'S	11:48 UT 98°30'E, 51°24'N	11:21 UT 113°18'E, 32°54'N

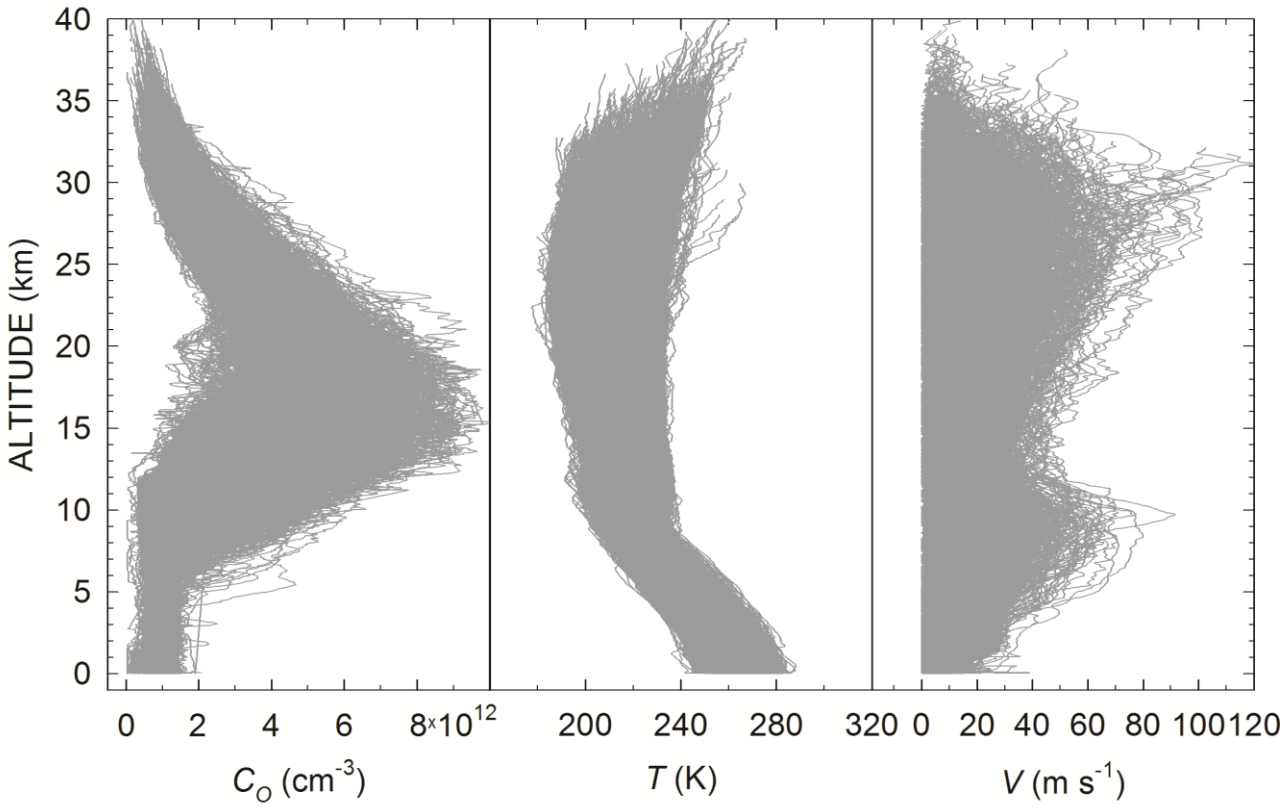

Fig. 1. Profiles of the ozone density C_O (left panel), temperature T (middle panel) and wind velocity V (right panel) subject of the analysis in the present research.

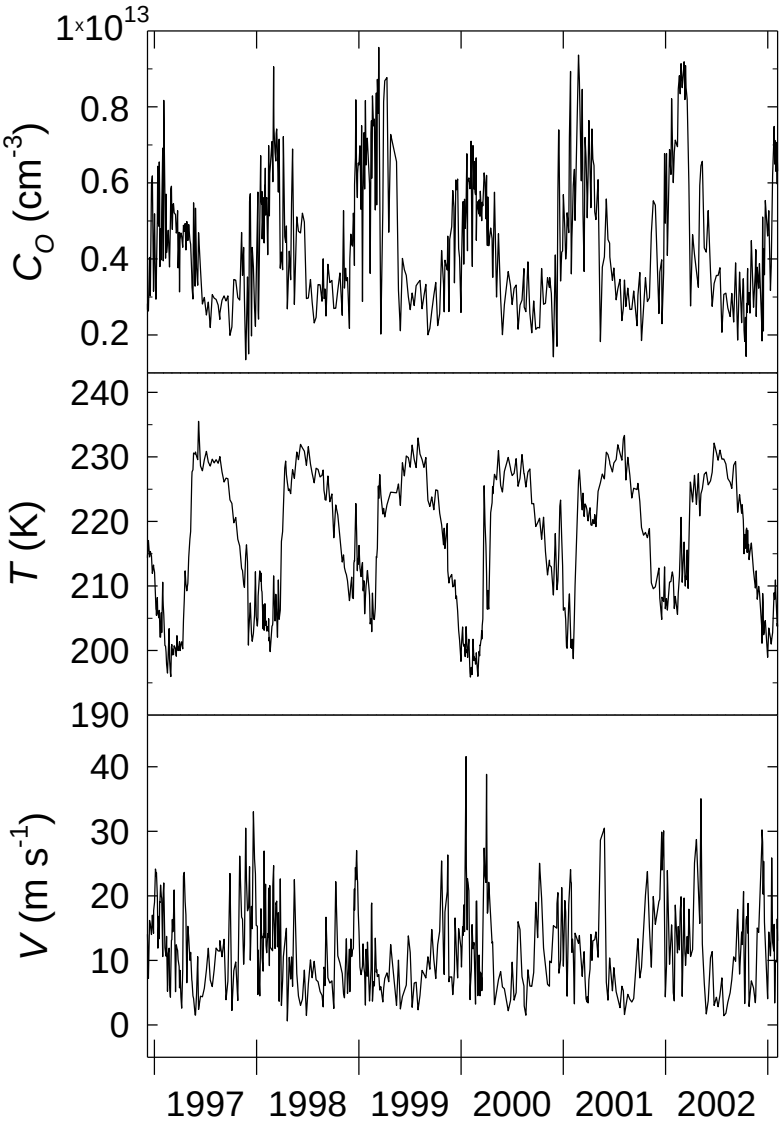

Fig.2. Segments of the three time series presenting the variability in ozone density C_O, temperature T and wind velocity V at 15 km altitude. A 6-year period, illustrating the time series was chosen to help for evidencing the corresponding short-period variations

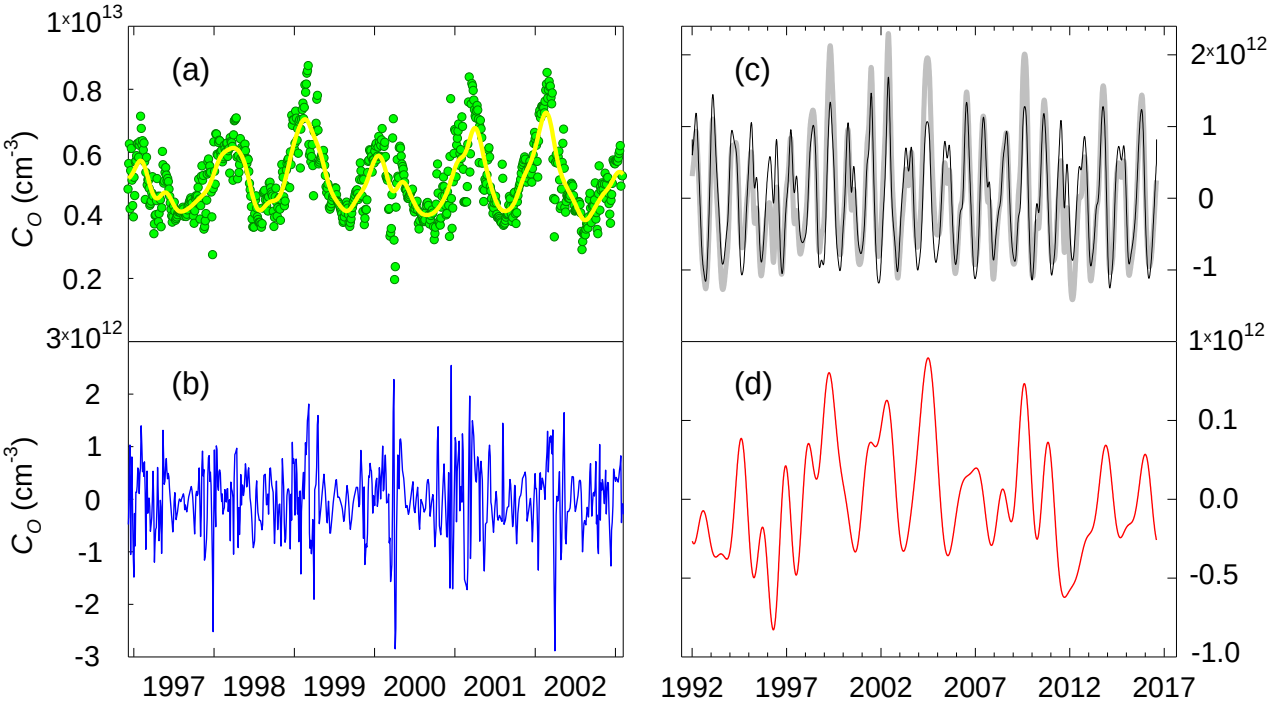

Fig. 3. An example that illustrates the separation of the IS and IA variations in the ozone density at 18 km altitude. The circles in panel (a) show the original data represented by the corresponding columns of **F′**, while the curve exhibits the long-period component retrieved by using a running average procedure over a 30-day window. Panel (c) presents the later component from which the linear trend was removed (grey curve) together with the variations composed by the periods not higher than one year (black curve). The differences between the two time patterns given in panels (a) and (c), which are shown in (b) and (d) respectively, are considered to represent the IS (b) and IA (d) variations in the ozone density. The time scales in both (a), (b) and (c), (d) panel pairs are chosen so that the details of the corresponding variation features can be clearly seen.

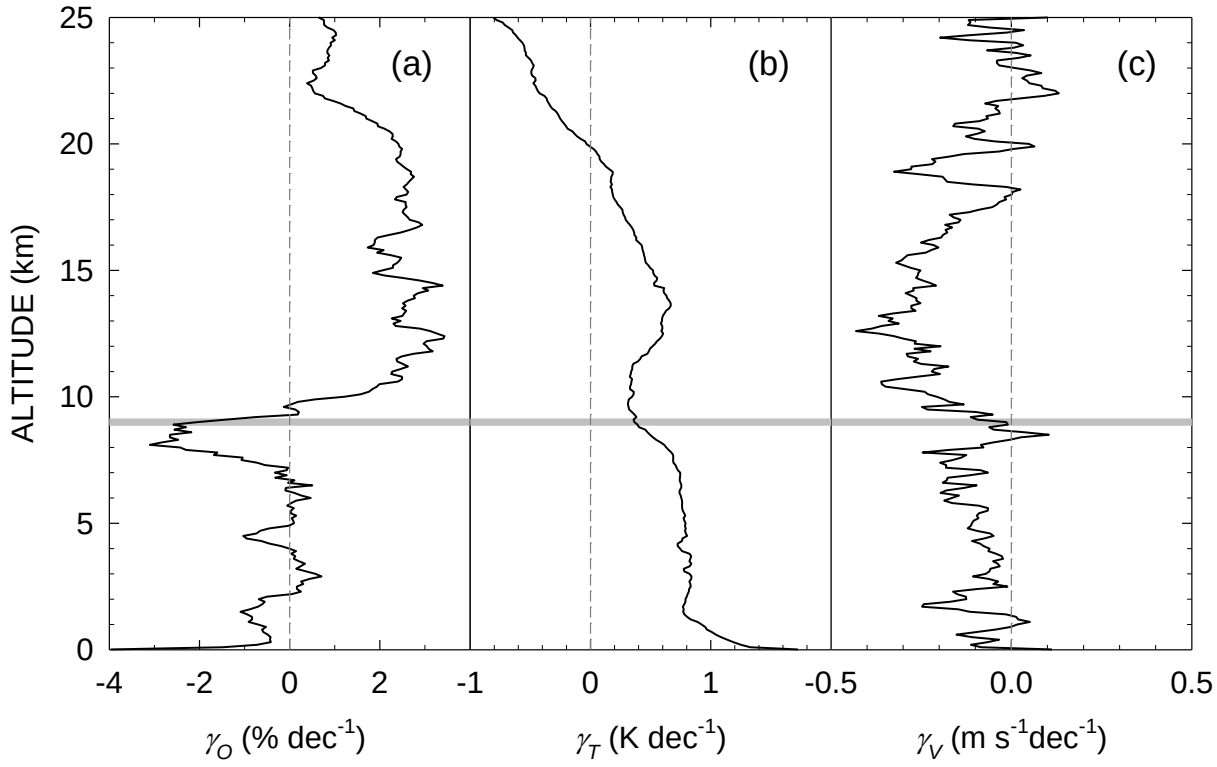

Fig. 4. Vertical distributions of the trends γ_O, γ_T, and γ_V obtained within 1992 – 2016 period for the ozone density C_O (a), temperature T (b) and wind velocity V (c), respectively as a result of the adopted procedure leading to the construction of the corresponding anomaly matrices. Vertical dashed lines indicate the zero value for each of the trends, while the thick horizontal grey line exhibits the mean level of the Svalbard tropopause evaluated from the soundings.

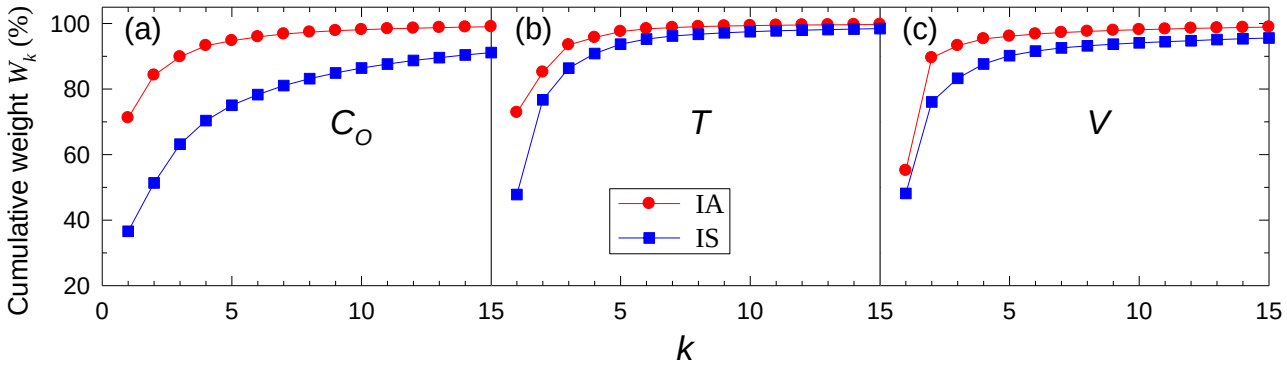

Fig. 5. The cumulative weight W_k of the (EOF, PC)$_{1\text{-}15}$ pairs obtained after decomposition of the matrices $\mathbf{F_{IA}}$ and $\mathbf{F_{IS}}$, constructed to represent the IA and IS variations in the ozone density C_O (a), temperature T (b) and wind velocity V (c), respectively.

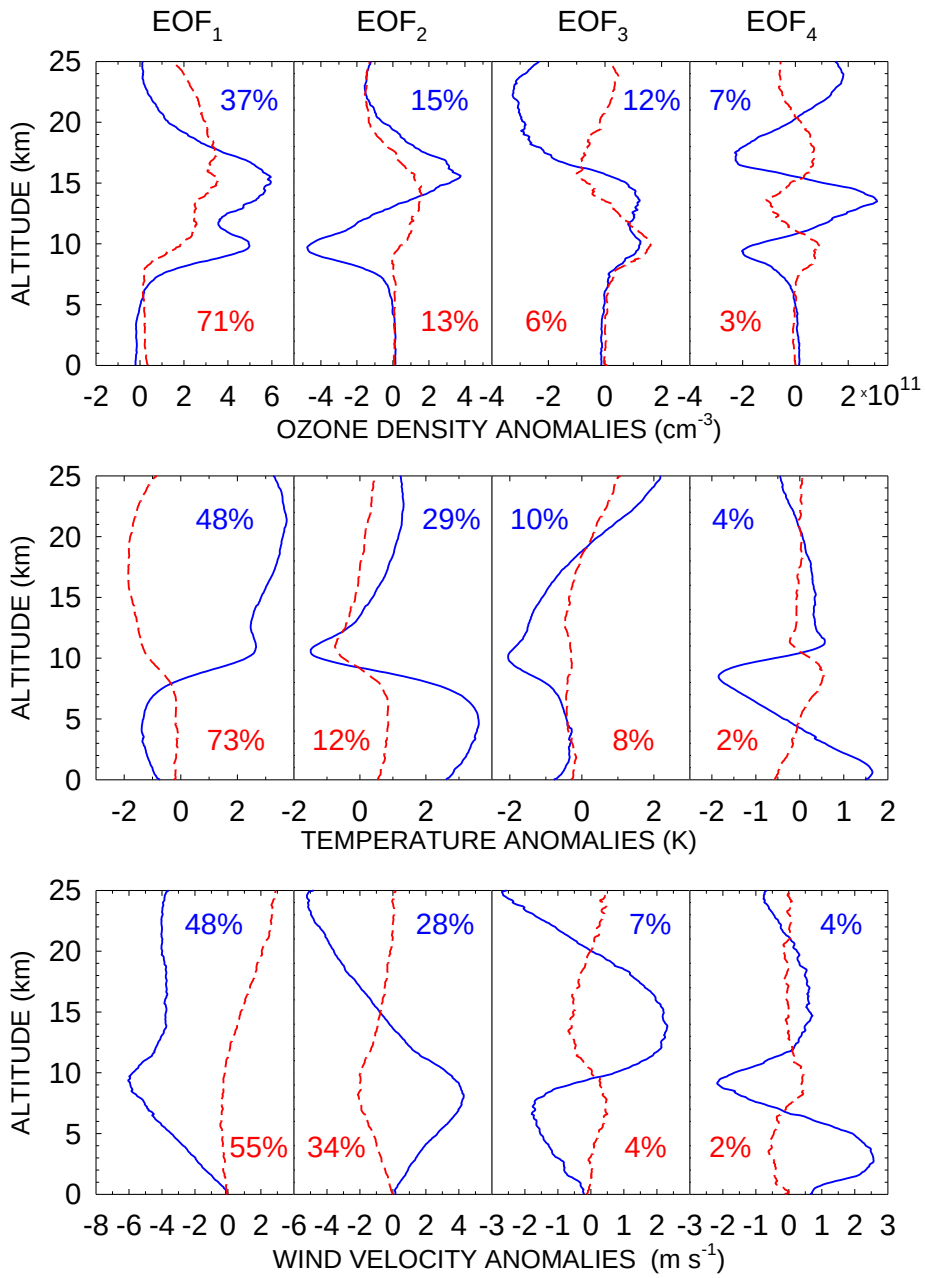

Fig. 6. The first four EOF components associated with the IS (solid curves) and IA (dashed curves) variations in the ozone (upper row), temperature (middle row) and wind velocity (lower row), found through decomposition of the anomaly matrices $\mathbf{F_{IS}}$ and $\mathbf{F_{IA}}$, respectively. The EOF weights, given in the panels are referred to IS (upper number) and IA (lower number) oscillations and each column of panels corresponds to the EOF_j indicated at the top of the figure.

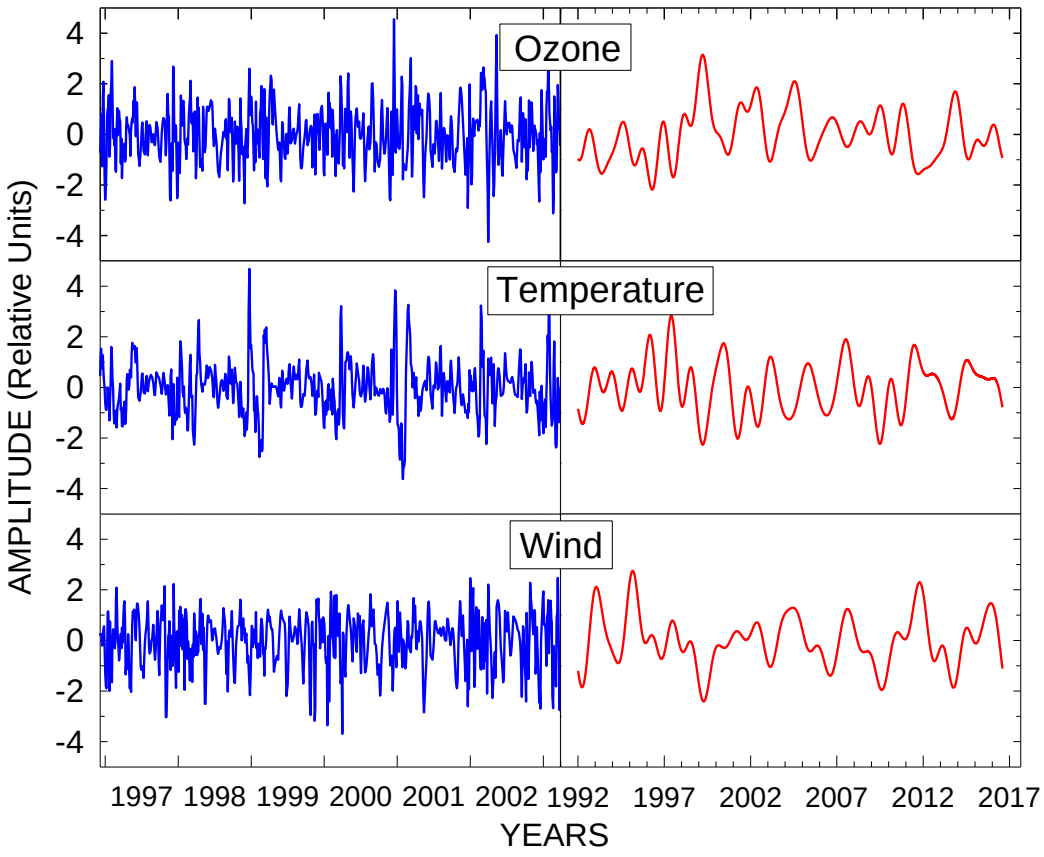

Fig. 7. PC_1 time series found for the IS (left) and IA (right) variations in the ozone density, temperature and wind velocity. A 6-year period was chosen for the IS variations in order to evidence better the high-frequency oscillations.

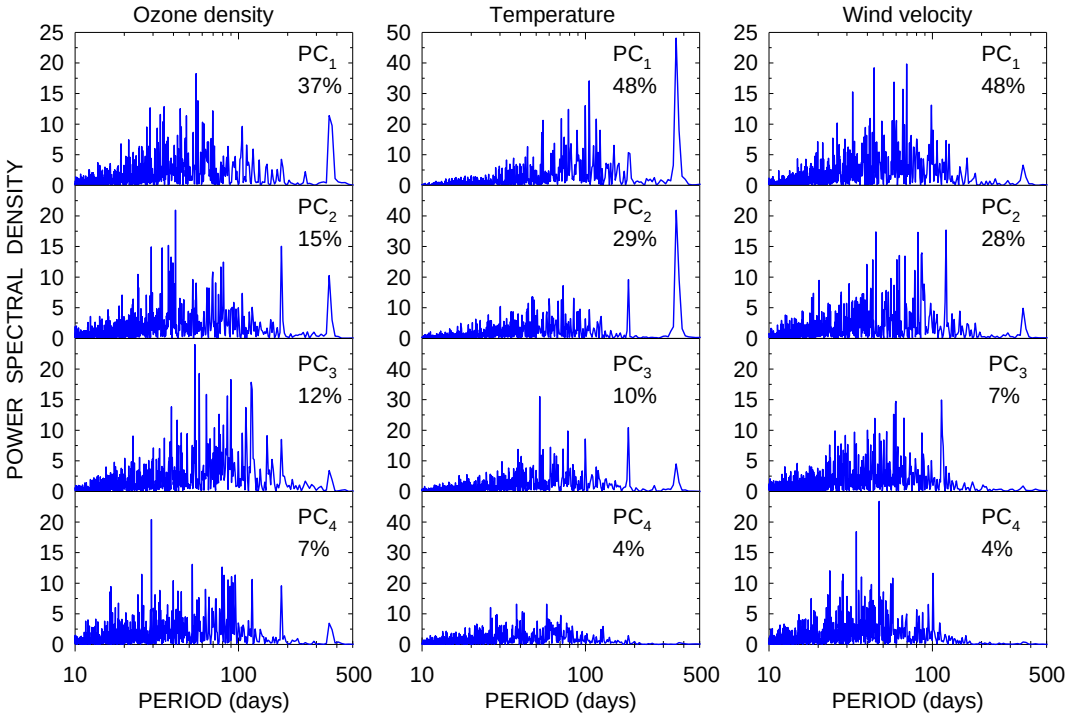

Fig. 8. Spectra of the first four PCs associated with the IS variations in the ozone density (left column), temperature (middle column) and wind velocity (right column), respectively. The PC number and its weight are indicated in each panel.

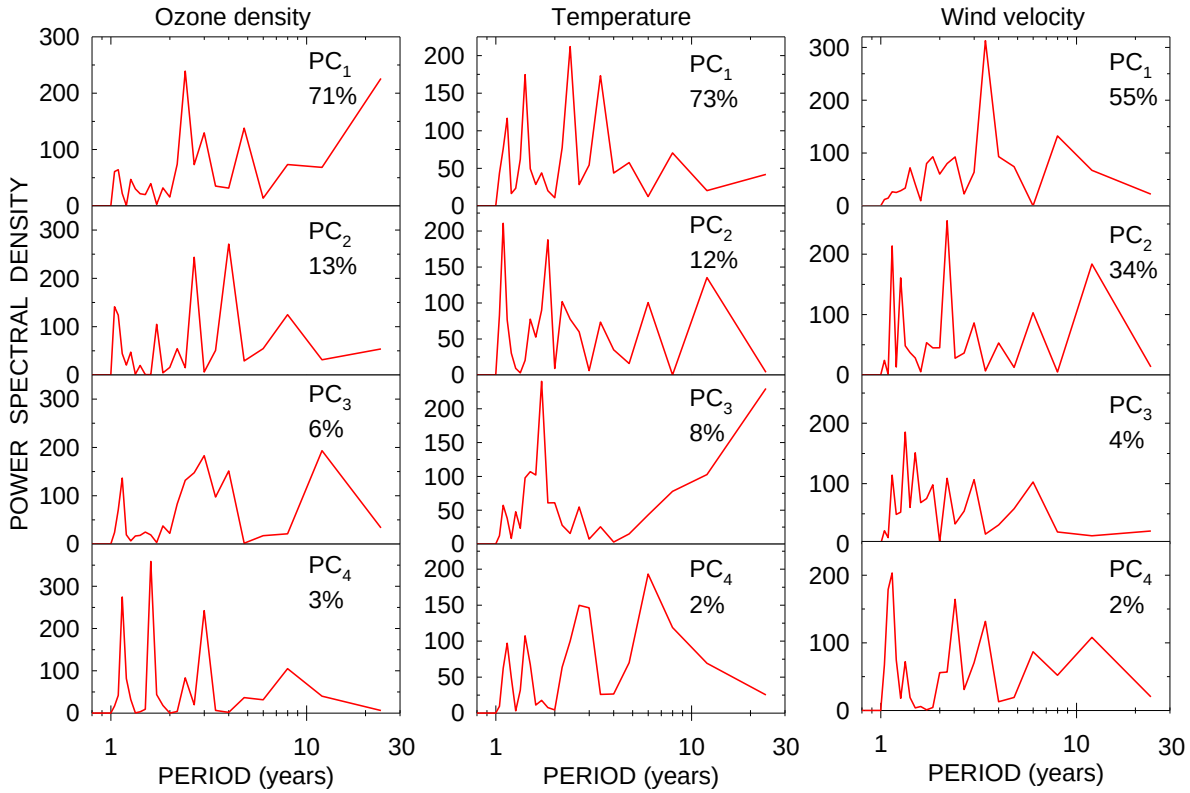

Fig. 9. Spectra of the first four PCs obtained for the IA oscillations in ozone density (left column), temperature (middle column) and wind velocity (right column). Similarly to Fig. 8 the PC number and weight are indicated in the corresponding panels.

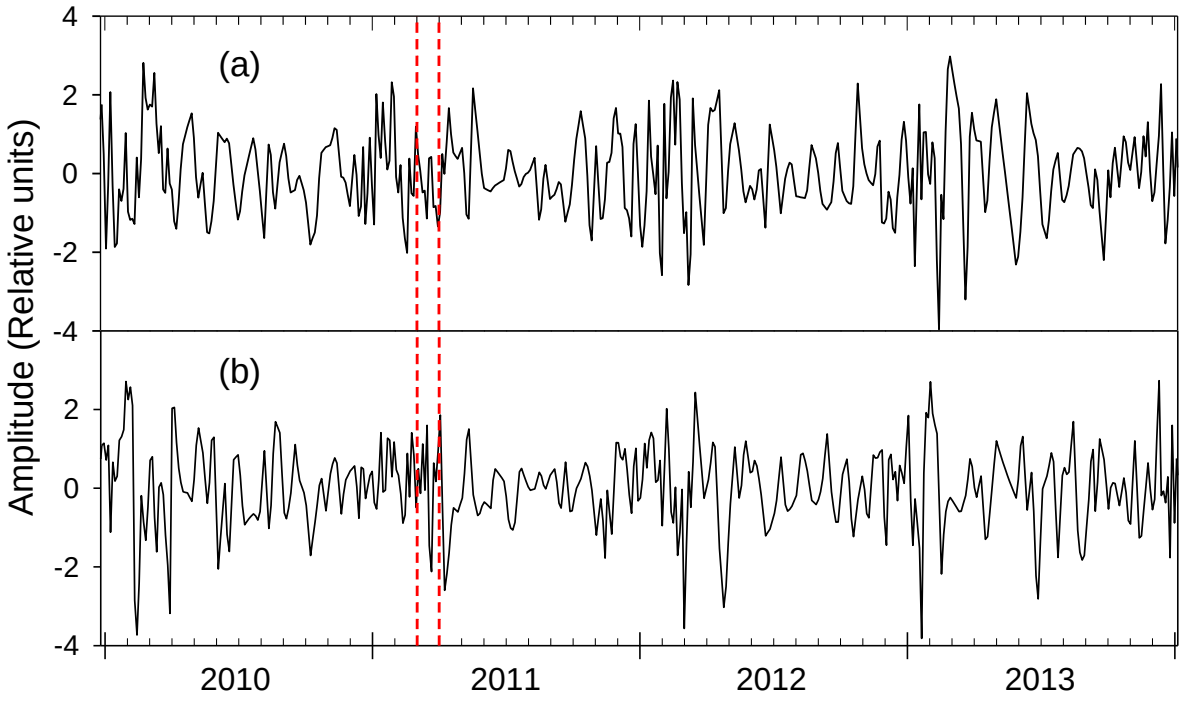

Fig. 10. Panel (a) exhibits the time patterns of the PC_1 associated with the IS variations in the ozone density over Svalbard for 2010 – 2013, while (b) shows the same for PC_2. The vertical dashed lines bound the period corresponding to March, 2011 when the strong ozone depletion event took place over Arctic.

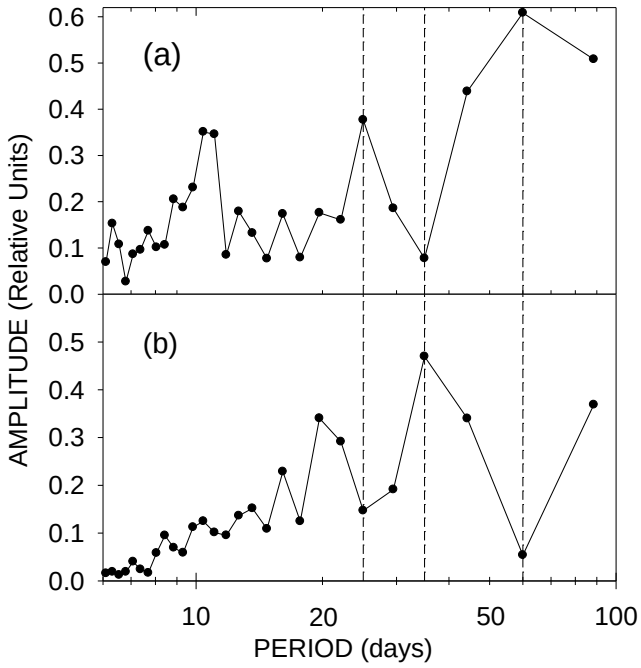

Fig. 11. The spectra of the PC_1 associated with the IS ozone density variations estimated for the 6-month periods from September 2010 to February 2011 (a) and from April to September 2011 (b), respectively. The vertical dashed lines indicate the spectral components peaked at 25-, 35- and 60-day periods

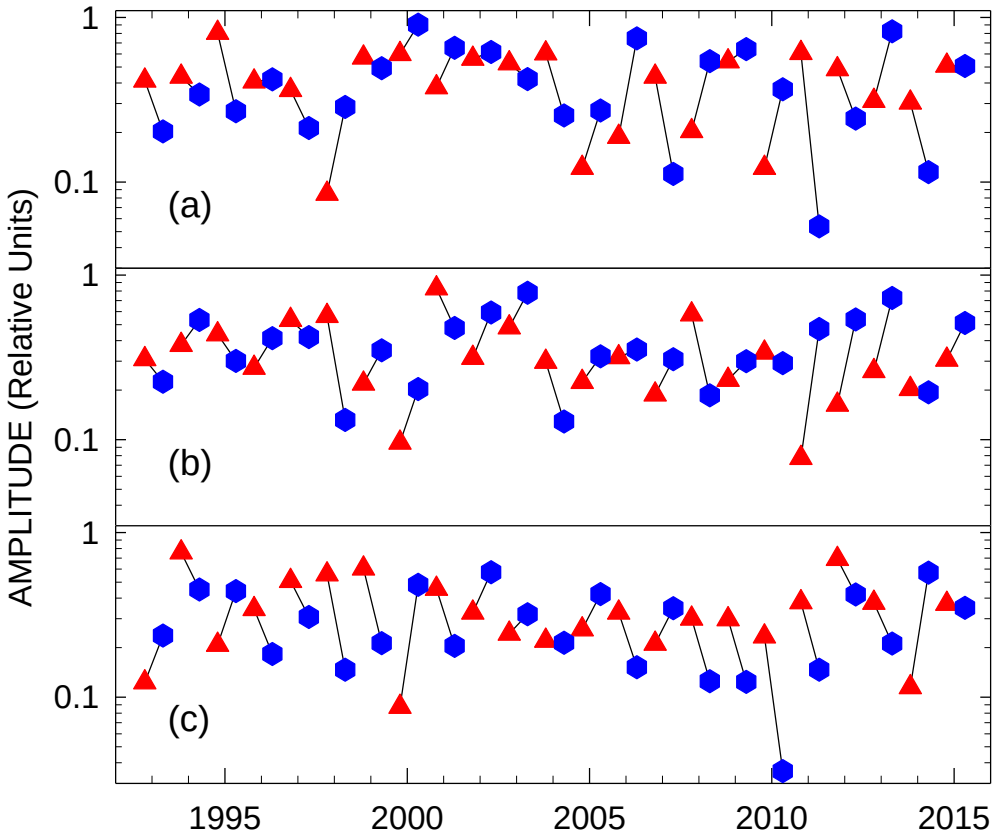

Fig. 12. Time patterns of the amplitudes $A_i'(p)$ (triangles) and $A_{i+1}''(p)$ (diamonds) of the PC_1 ozone oscillations evaluated for the spectral components peaked at periods of p = 60 (a), p = 35 (b) and p = 25 days (c). The lines that connect the corresponding amplitudes represent the discrepancies $|A_i'(p) - A_{i+1}''(p)|$, which give an idea about the changes in the amplitudes of the selected harmonics passing from T_i' to T_{i+1}'' for each year.

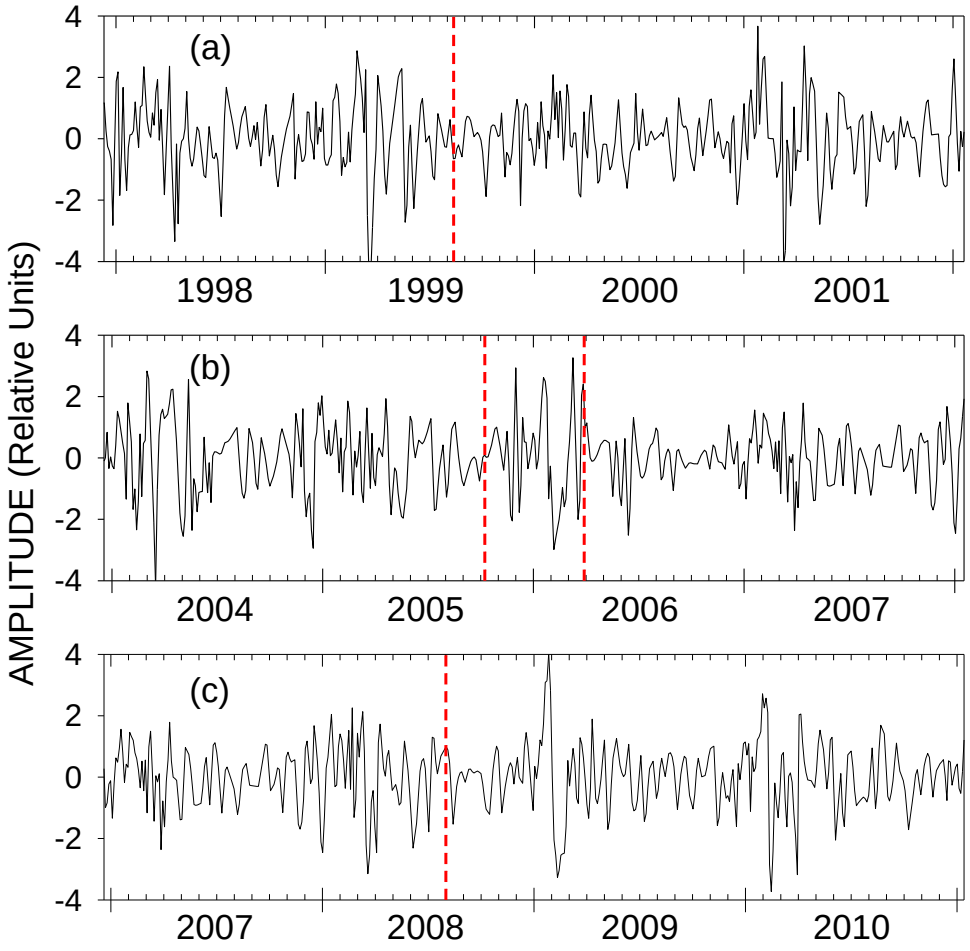

Fig. 13. Time patterns of the PC_2 associated with the IS ozone variations during the periods containing the solar eclipses on 11 August 1999 (a), 3 October 2005 and 29 March 2006 (b), and 1 August 2008 (c), which days are indicated by vertical dashed lines in each of the panels.

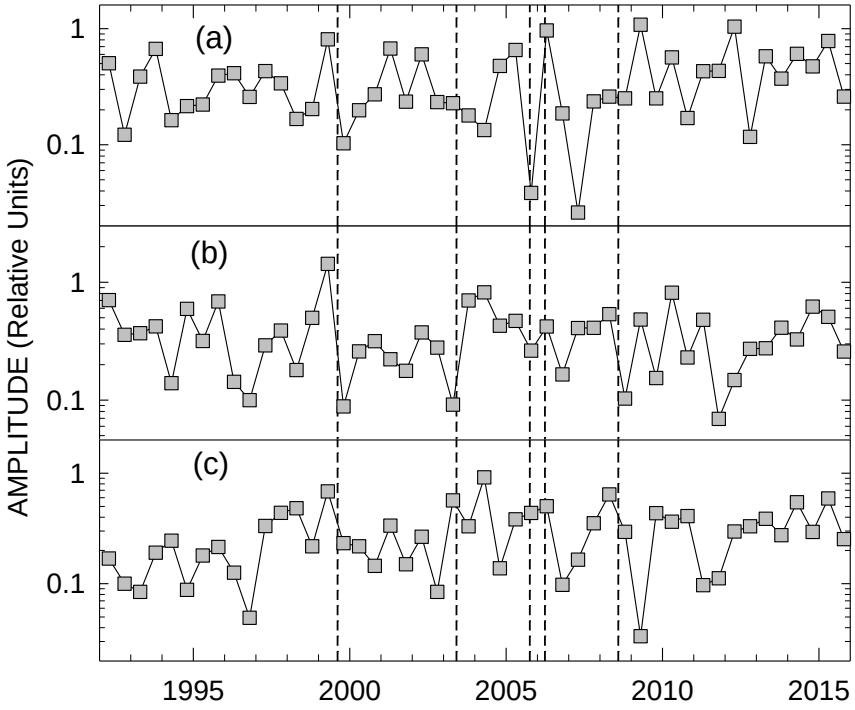

Fig. 14. Variations in the amplitude of 60-day (a), 35-day (b) and 25-day (c) harmonics characterising the PC_2 IS ozone oscillations evaluated for the first and second 6-month time-intervals of each year pertaining to the period under study and indicated by grey squares. The vertical dashed lines mark the occurrences of solar eclipses listed in Table 2.